Received: 10 10 2025 | Revised: 12 03 2026 | Accepted: 11 04 2026
DOI: 10.15294/jim.v8i1.32000
Page 28 – 40

JIM: Jurnal Inovasi Mesin

Optimization and Comparison of Linear and Curved Cone Contraction Designs Using the CFD Method for the Development of a Two-Dimensional Low-Subsonic Wind Tunnel

Sulthan Dzaki A[1*], Hendrix Noviyanto Firmansyah[1], Samsudin Anis[1].

1 Department of Mechanical Engineering, Faculty of Engineering, Universitas Negeri Semarang, Indonesia
*sulthan_d_ahmada@students.unnes.ac.id

Keywords:
Wind tunnel
CFD
Contraction cone
Flow
Aerodynamics

Abstract
The geometry design of the contraction cone plays an important role in determining the flow performance in a subsonic wind tunnel. This study aims to examine and compare two forms of contraction cone design, namely the linear model and the polynomial curve, in the development of a two-dimensional Low Subsonic Wind tunnel using the Computational Fluid Dynamics (CFD) numerical simulation method. The main objective of this study is to evaluate the effect of geometric shapes on velocity distribution, flow uniformity, and aerodynamic performance in the test chamber. Simulations were carried out using ANSYS Fluent software with the k-ω SST turbulence model, and the NACA 4412 airfoil was used as a test object to observe the aerodynamic forces. The simulation results show that the contraction cone with the polynomial curve design produces a more uniform flow, higher speed, and a better lift coefficient (Cl) than the linear design. In addition, the curve design is also able to suppress flow disturbances such as flow separation and boundary layer effects. Based on these findings, the contraction cone with a polynomial curve profile is more recommended for application in a two-dimensional subsonic wind tunnel to improve the efficiency and accuracy of aerodynamic testing.

1 *Introduction*

Aerodynamic testing requires controlled flow conditions that are representative of real-world phenomena. One commonly used experimental device for this purpose is a wind tunnel, which allows for the visualization and quantification of fluid flow characteristics relative to an object. In subsonic wind tunnel systems, the geometric design of the contraction cone is a crucial component determining the flow quality in the test section. The primary role of the contraction cone is to increase fluid velocity while simultaneously stabilizing the flow to near-ideal conditions before entering the test chamber. Therefore, the contraction cone design must be able to minimize disturbances such as turbulence, uneven velocity distribution, and flow separation.

ISSN 2746-7694

In general, contraction cones can be designed with either a linear or polynomial wall profile. Previous studies have shown that the polynomial profile has better potential for maintaining flow uniformity and suppressing boundary layer effects than the linear design. However, implementation and production complexity often hinder its implementation, particularly at the laboratory scale.

This study aims to compare the performance of two contraction cone designs—linear and polynomial—through a numerical simulation approach using the Computational Fluid Dynamics (CFD) method. By referring to parameters such as velocity distribution, pressure, and aerodynamic force characteristics, an evaluation is conducted to determine the most optimal design to support testing in a two-dimensional Low Subsonic Wind Tunnel. The findings of this study are expected to contribute to the development of efficient and economical wind tunnel designs, as well as being relevant for research and learning needs in the fields of mechanical engineering and aerodynamics.

2 *Research Methods*

2.1 Geometri

The wind tunnel geometry was created in 2D with an inlet of 600 × 700 mm and an outlet of 200 × 300 mm (ratio 1:7). Two contraction cone models were used: linear and 6th order polynomial curves. Simulations were performed using ANSYS Fluent 2023 R1. Water was used as the incompressible fluid, with a maximum inlet velocity of 50 m/s. A NACA 4412 airfoil was installed in the test section for force coefficient testing.

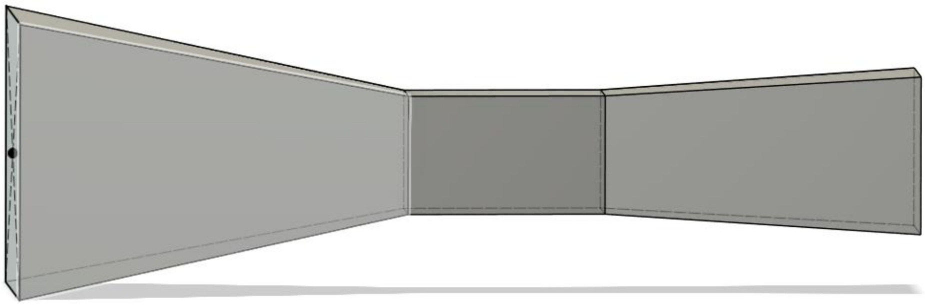

(a)

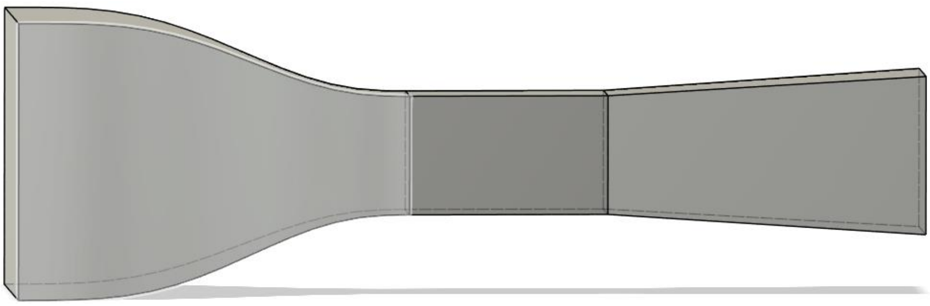

(b)

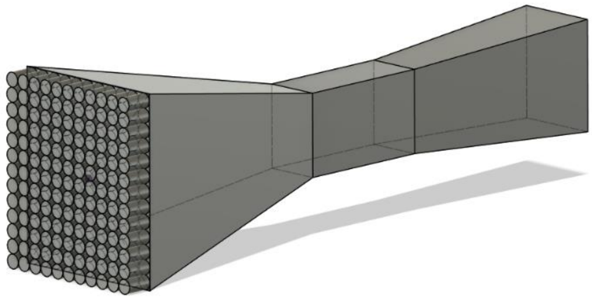

(c)

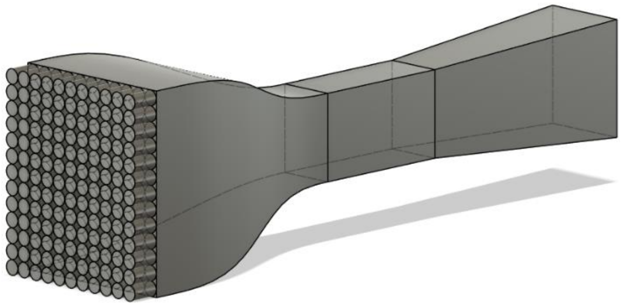

(d)

Figure 1. Simulation Geometry of Wind tunnel

(a) Wind tunnel with contraction cone linear, (b) Wind tunnel with curve contraction cone, (c) Wind tunnel linear with honeycomb, dan (d) Wind tunnel kurva with honeycomb

2.2 Drag and Lift

In aerodynamics, there are two forces that affect an object while it is in the air, namely drag and lift. Drag is a force that results from the interaction between the surface of an object and the fluid flowing around it, which force is always opposite to the direction of motion of the object [1-5]. Drag occurs due to a combination of fluid friction with the surface of the object and the pressure caused by differences in flow speed around the object. Factors that affect drag are the drag coefficient (Cd), flow velocity (V), fluid density (ρ), and the surface area exposed to the fluid.

The drag equation is written as follows in Eq. (1).

$$D = \frac{1}{2} C_d \rho V^2 A \quad (1)$$

Where:

D = drag (N)

C_d = drag coefficient

ρ = fluid density (kg/m^3)

V = fluid velocity (m/s)

A = frontal surface area of an object (m^2)

The lift equation is written as follows in the Eq. (2).

$$L = \frac{1}{2} C_l \rho V^2 A \quad (2)$$

Where :

L = lift (N)

C_l = lift coefficient

ρ = fluid density (kg/m³)

V = fluid flow (m/s)

A = wing surface area (m²)

The wing surface area has the following formula in the Eq. (3).

$$A = b \times c \quad (3)$$

Where :

b = Wingspan (m)

c = Chord Length (m)

2.3 Mach number

Mach number is a parameter in fluid mechanics and aerodynamics that is used to describe the speed of a fluid flow relative to the speed of sound [6-8]. Mach number is expressed in the following formula in the Eq. (4).

$$M = \frac{V}{c} \quad (4)$$

Where,

M = Mach number

V = Fluid flow (m/s)

c = The speed of sound in the medium (m/s)

The formula for the speed of sound can be calculated using the Eq. (5)

$$c = \sqrt{\gamma R T} \quad (5)$$

Where :

γ = Specific heat capacity ratio (1.4 for air at standard conditions)

R = Ideal gas constant (28 J/kg*K for the air)

T = Absolute temperature of the medium (Kelvin, K)

2.4 Reynolds number

The Reynolds number is a dimensionless parameter in fluid mechanics that is used to determine the type of fluid flow, whether it is laminar, transitional, or turbulent. This number describes the ratio between inertial forces and viscous forces in a flowing fluid [9-11]. The formula for determining the Reynolds number is written as follows in the Eq. (6).

$$Re = \frac{\rho V L}{\mu} = \frac{VL}{\nu} \quad (6)$$

Where,

Re = Reynolds number

ρ = Fluid density (kg/m^3)

V = Fluid flow (m/s)

L = Characteristic length or typical dimension of an object (m)

μ = Dynamic viscosity of fluid (Pa*s or N*s/m^2)

ν = Kinematic viscosity (m^2/s), with $\nu = \frac{\mu}{\rho}$

The Reynolds number determines the type of fluid flow, which is then categorized into 3 types of flow in general, namely laminar flow which has a Reynolds number value below 2000, transition flow which has a Reynolds number value between 2000 and 4000, and turbulent flow which has a Reynolds number value above 4000.

2.5 Hydraulic Diameter

In fluid mechanics, particularly in internal flow in non-circular channels, the concept of hydraulic diameter (Dh) is used as a characteristic length to analyze and compare flow performance with standard circular channels. Hydraulic diameter is used for correlations and equations developed for circular pipes in channels with non-circular cross-sections, such as rectangular channels or channels with other complex shapes.

By definition, the hydraulic diameter is four times the cross-sectional area of the flow divided by the wetted circumference of the channel. The wetted circumference (P) is the length of the channel surface that is in direct contact with the flowing fluid. The general formula for calculating hydraulic diameter is shown in the Eq. (7).

$$D_h = \frac{4A}{P} \quad (7)$$

Where:

D_h = Hydraulic diameter (m)

A = Flow cross-sectional area (m^2)

P = Wet around (m)

For different cross-sectional shapes, the calculation of A and P will vary. For example for circular pipes. The hydraulic diameter is equal to the actual diameter of the pipe. ($D_h = D$), cause $A = \pi D^2/4$ and $P=\pi D$. For rectangular channels (fully filled): If h is the height and w is the width of the channel, then $A = h\times w$ and $P = 2(h+w)$. Thus, $D_h = \frac{4(h\times w)}{2(h+w)} = \frac{2hw}{(h+w)}$.

2.6 CFD *(Computational Fluid Dynamics)*

Potter et al., in their book, "Mechanics of Fluids," explain that there are three basic laws of fluid mechanics: conservation of mass, conservation of momentum, and conservation of energy. The law of conservation of mass (the Continuity Equation) states that the mass of fluid entering a system must equal the mass leaving it, unless there is an accumulation of mass within the system. The differential equation is written as follows in the Eq. (8).

$$\frac{\partial \rho}{\partial t} + \nabla \cdot (\rho V) = 0 \qquad (8)$$

Where:

ρ = Fluid density (kg/m^3)

t = time (s)

V = fluid velocity vector (m/s)

$\nabla\cdot$ = divergence operator

If the fluid is considered incompressible as seen in the Eq. (9).

$$\nabla \cdot (V) = 0 \qquad (9)$$

Which means the fluid velocity must keep the flow constant. The law of conservation or conservation of momentum (Navier-Stokes equation) is an application of Newton's second law, which states that changes in the momentum of a fluid in a system occur due to external forces acting on the fluid. The differential equation is written as follows in the Eq. (10).

$$\rho(\left(\frac{\partial V}{\partial t}\right) V \cdot \nabla V) = -\nabla P + \mu \nabla^2 V + \rho g \qquad (10)$$

Where :

V = fluid velocity vector (m/s)

t = time (s)

$\nabla\cdot$ = divergence operator

ρ = Fluid density (kg/m^3)

P = Pressure (Pa)

μ = dynamic viscosity (Pa·s)

g = acceleration due to gravity (m/s^2)

The equation written describes the change in fluid velocity that is influenced by pressure, viscosity, and other external forces.

3 *Result and Discussion*

3.1 Result of Mesh Wind Tunnel

The mesh is automatically generated by Ansys Meshing in the Fluent system, and the mesh quality is then checked using the mesh quality table provided. The meshing results for each model are shown in the following image.

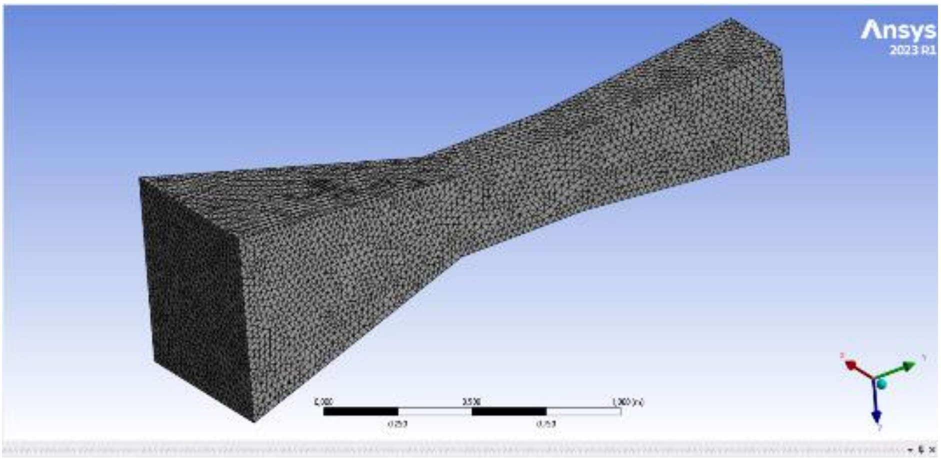

(a)

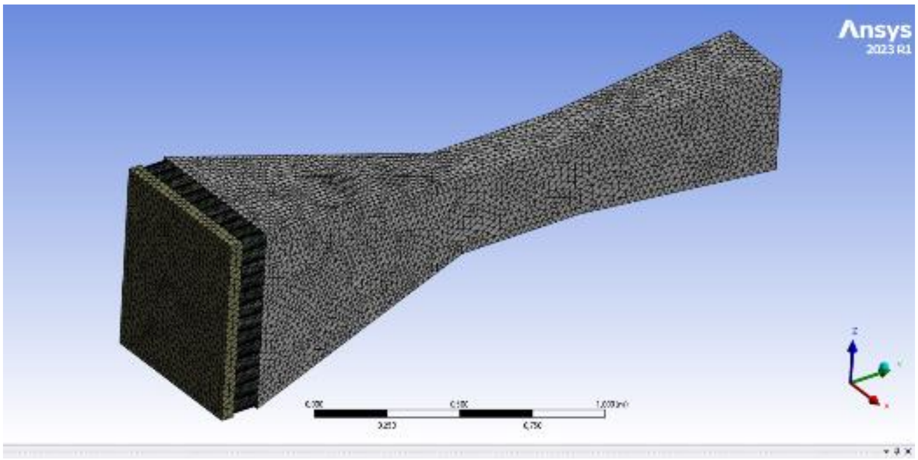

(b)

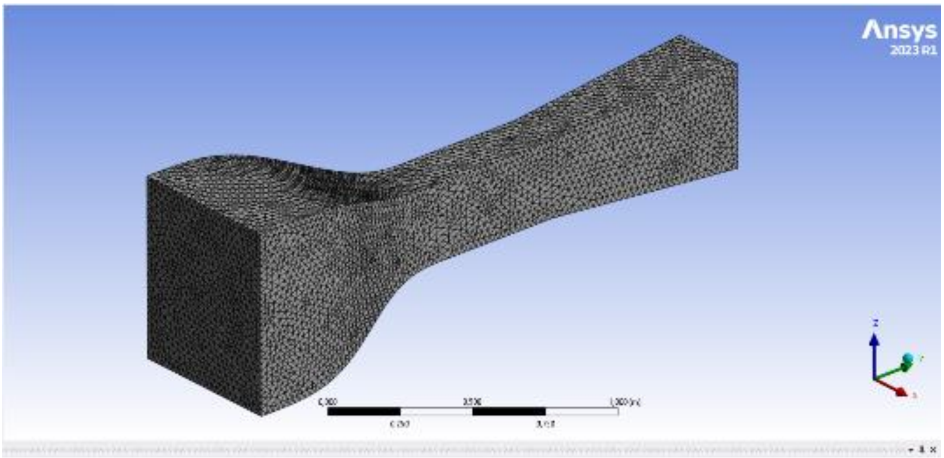

(c)

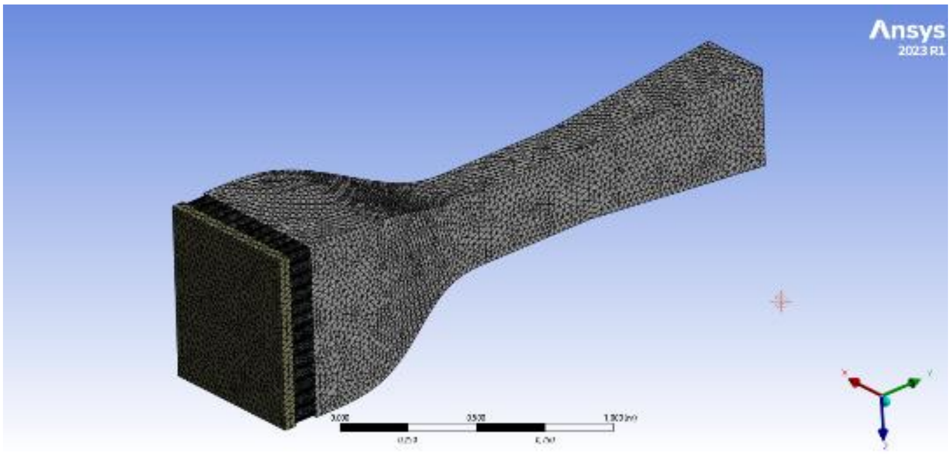

(d)

Figure 2. Mesh Results of Wind tunnel

(a) Mesh WT Linear, (b) Mesh WT Linear Honeycomb, (c) WT Curve

dan (d) WT Honeycomb Curve

The mesh quality based on the skewness value in the mesh indicates the skewness criteria as a determinant of mesh quality. The maximum skewness value is <1, and the best value is <0.25, which is excellent. The skewness values and model criteria are presented in the following table.

Table 3. 1 WT Mesh Quality Table (Based on Previous Design)

Quality of mesh parameters	Value
Skewness	0.2 (modus)
Minimum	2.5903e-006
Maximum	0.79869
Average	0.25326
Standard Devaition	0.12736
Nodes	141130
Elements	652970

3.2 Mesh Independence Study

The global mesh element applied to the modeling of the four geometric designs is based on previous research by Firmansyah and Wiraardi (2023), which is 25 mm. The following are the mesh results for each model with a mesh element size of 25 mm.

Table 3. 2 Table of Geometric Mesh

Variations	Nodes	Skewness
WT Linear	33236	0.2
WT Linear Honeycomb	137599	0.2
WT Curve	23005	0.2
WT Honeycomb Curve	141130	0.2

From the meshing results, it can be seen that all mesh qualities of each model are sufficient to proceed to the next process.

3.3 **Wind Tunnel Test Data Validation**

The purpose of data validation is to compare the results of mathematical calculations with the results of simulations that have been run. Mathematical calculations are an approach that calculates ideal possibilities in the real world, while simulation results need to be compared with the continuity equation to prove whether the simulation results are similar or match the ideal conditions or not. Data validation was carried out on three models that are developments of an initial model that was used as a reference. The following table compares one reference design with three other development designs.

Table 3.3 Validation of Simulation Data and Calculation of Equations as a Comparison

Model variations	Speed Test Point Test Section (m/s)			Means (m/s)	Error (%)
WT Linear *Honeycomb*	35.088200	35.343106	35.391074	35.274127	0.7832%
WT Linear	35.040467	35.302269	35.353317	35.232018	0.6629%
WT *Honeycomb Curve*	35.266253	35.388650	35.428460	35.361121	1.0318%
WT Curve	35.109586	35.279350	35.338131	35.242356	0.6924%
Equation Calculation	35				

The model constructed as a reference model is the WT (Wind tunnel) Linear as shown in Table 3.3. Other models created are the WT Linear Honeycomb, WT Curve Honeycomb, and WT Curve. In the calculation of the equation carried out, namely finding the velocity at the outlet contraction cone or inlet test section, the equation $A1 \times V1 = A2 \times V2$ is used so that the velocity at the outlet contraction cone or inlet test section is 35 m/s. Using a comparison between the results of the model simulation and the calculation of the equation, the error figures are all below 5% [12-16]. The errors obtained indicate that the simulation of the wind tunnel models has been made according to the requirements to describe actual conditions.

3.4 Air Speed in Wind Tunnel

The data from the CFD simulation process for the four geometry models using ANSYS 2023 R1 shows velocity points at 27 measurement points, as an observation of fluctuations that occur during fluid flow through the geometry. Data from the velocity points are presented in the following table.

Table 3.4 Air Speed Data at 27 Measurement Points

Model variations	Speed testing point (m/s)								
	Contraction Cone			Test Section			Diffuser		
	1	2	3	4	5	6	7	8	9
WT Linear *Honeycomb*	6,6328	10,3614	17,6133	35,0882	35,3431	35,3911	29,8780	25,3961	22,2196
WT Linear HC point a	6,8127	10,5242	17,6732	35,2868	35,4205	35,4831	29,8440	25,5590	22,2337
WT Linear HC point b	6,8493	10,7170	18,1416	35,2595	35,4473	35,5254	29,9036	25,4621	22,2658
WT Linear	6,4439	10,2535	17,5291	35,0405	35,3023	35,3533	29,8275	25,3303	22,1408
WT Linear point a	6,5150	10,3944	17,6014	35,2439	35,3845	35,4536	29,8053	25,5076	22,1700
WT Linear point b	6,6634	10,5974	18,0596	35,2186	35,4027	35,4865	29,8599	25,4046	22,1924
WT *Honeycomb Curve*	5,7407	9,3293	21,5403	35,2663	35,3887	35,4285	29,9200	25,3405	22,3216
WT *Honeycomb Curve point a*	5,5154	9,1400	21,9074	35,2949	35,4221	35,4980	29,6962	25,3576	22,3699
WT *Honeycomb Curve point b*	5,6210	8,9687	21,9108	35,3001	35,4057	35,4711	29,8096	25,4115	22,3056
WT Curve	5,6669	9,3922	22,3408	35,1096	35,2794	35,3381	29,9459	25,3296	22,2334
WT Curve point a	5,4278	8,7058	22,1945	35,2410	35,3873	35,4825	30,1149	25,4642	22,1561
WT Curve point b	5,4728	9,1201	21,6599	35,2235	35,3461	35,4614	29,4620	25,5786	22,3714

In the WT Linear Honeycomb design scope, the highest speed point is at sub-point 6b, where the speed reaches 35.5254 m/s, while the lowest speed is at point 1, with a speed of 6.6328 m/s. In the WT Linear design scope without Honeycomb, the highest speed point is at sub-point 6b, where the speed reaches 35.4865 m/s, while the lowest speed is at point 1 with a speed of 6.4439 m/s. There is an increase in speed in the WT Curve Honeycomb design, with the highest speed reaching 35.4980 m/s at sub-point 6a, and the lowest speed is at sub-point 1a, which is 5.5154. Finally, the WT Curve design without Honeycomb has the highest speed at sub-point 6a, which is 35.4285 m/s at sub-point 1a, which is 5.4278 m/s.

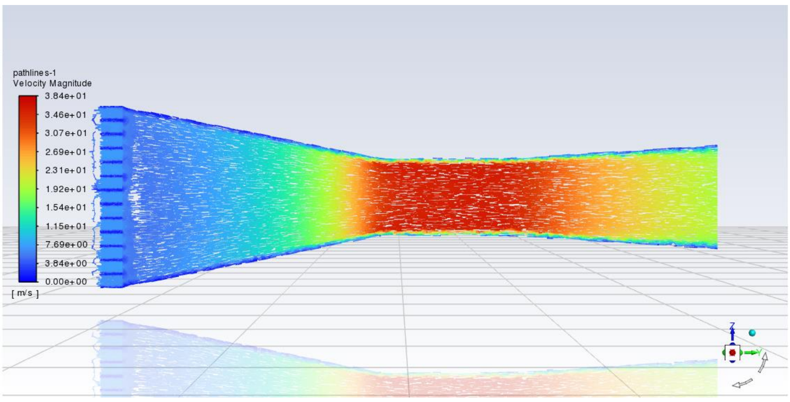

(a)

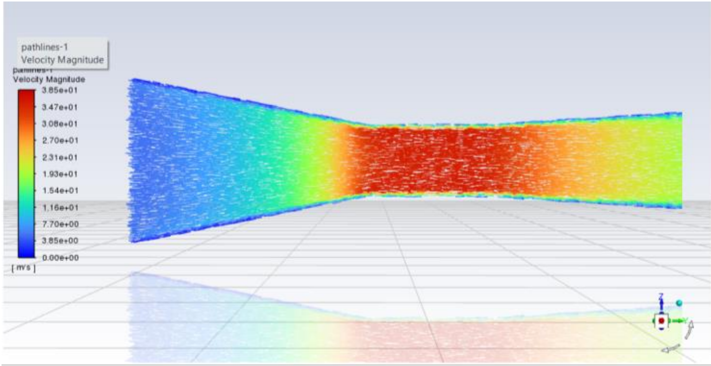

(b)

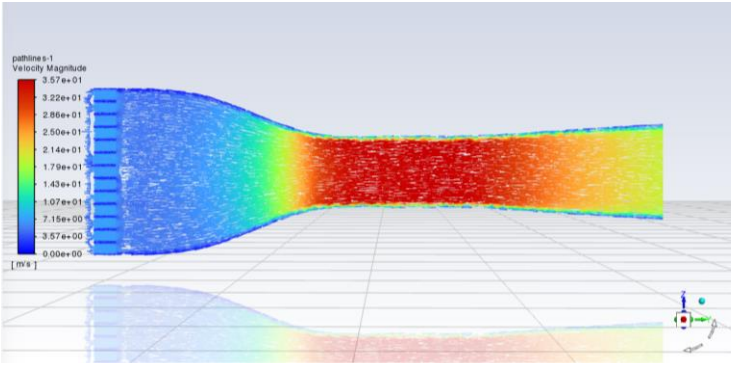

(c)

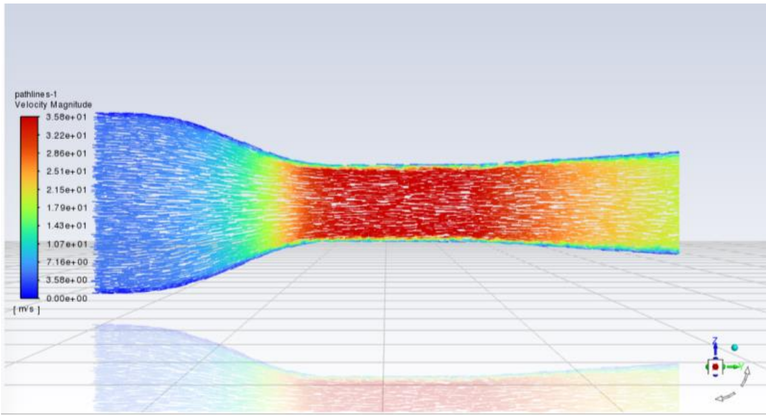

(d)

(a) WT Linear Honeycomb Velocity Contour, (b) Linear WT Velocity Contour, (c) WT Velocity Contour Honeycomb Curve, dan (d) WT Speed Contour Curve

Figure 3. Air velocity in wind tunnel

In line with the statement of M. Ali and K. Javed (2014), that acceleration occurs in the test section due to contraction constriction, but this is also caused by the contour or shape of the contraction cone itself, whether it is linear or has a curve. In Figure 3 and Table 3.4., namely the velocity contour on the Linear WT, it can be seen that the value of the resulting velocity in the test section is lower, namely 35.3023 m / s at point 5 compared to the curve design provided by Honeycomb in Figure 3, and the recorded speed is 35.3887 m / s at point 5. Thus, in terms of performance, the WT Curve with Honeycomb is better in terms of fluid acceleration compared to the Linear WT. The higher the speed that can be achieved by a wind, the higher the level of flow uniformity that can be achieved. [17].

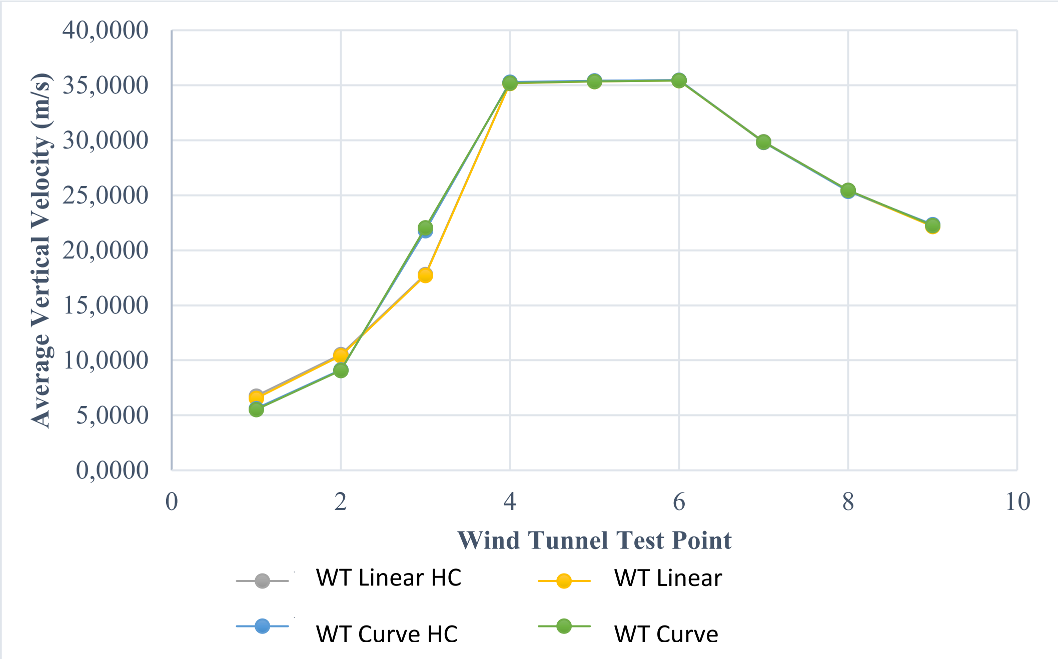

Figure 4. Airspeed Graph at 27 Points in 4 Geometry Variations

The differences in flow velocity distribution and velocity in the test section in each model variation indicate that the addition of honeycomb as a rectifier has a crucial function (Panda et al., 2016), so that when the flow first enters the contraction cone there is no turbulence. All test points have their peaks in the test section. [18-19].

4. *Conclusion*

Based on the results of simulation tests using the Computational Fluid Dynamics (CFD) method of the four variations of wind tunnel geometry, as well as testing the NACA 4412 airfoil with an aspect ratio of 7: 1 (wingspan versus chord length) in the test section with an angle of attack of 0°, the following conclusions can be drawn as The simulation results that have been carried out with the four wind tunnel geometry models show that although there are slight differences with the original design, it shows that the wind tunnel geometry design with a curve contraction cone profile can be used as an option for developing a wind tunnel with its honeycomb. There was a significant increase in negative pressure in the test section of the wind tunnel contraction curve with honeycomb. This increase in pressure greatly affects the uniformity of the flow passing through the test section. Tests with the honeycomb curve wind tunnel geometry containing the NACA 4412 airfoil with an angle of attack of 0° in it, showed that there was no vortex or wake region as a result of the boundary layer effect visually. This indicates that the speed and pressure achieved in the test section are ideal enough to be implemented. The difference between the NACA 4412 airfoil in the test section (internal flow) and the NACA 4412 airfoil in the open air (external flow) is the difference between the lift and drag forces generated. The lift and drag forces on the airfoil in the test section are greater than the lift and drag forces on the airfoil in the external flow. This indicates that there is a wall blockage effect that affects the test performance of the NACA 4412 airfoil in the test section of the wind tunnel caused by the insufficient hydraulic diameter.

References

1. Aerodynamics -- L_ J_ Clancy -- Pitman aeronautical engineering series, New York, 1975 -- John Wiley & Sons, Incorporated -- 9780273011200 -- 6f2d7b0c9841f40064879cfab586d3cd. (1975).
2. Alya Rahmadani Harahap, & Yahfizham Yahfizham. (2023). Algoritma Pemrograman Numerik Sebagai Solusi Efisien dari Permasalahan Matematika Kompleks. Jurnal Arjuna : Publikasi Ilmu Pendidikan, Bahasa Dan Matematika, 1(6), 12–20. https://doi.org/10.61132/arjuna.v1i6.284
3. Anderson, J. D., & Christopher Cadou, J. P. (2024). This International Student Edition is for use outside of the U.S.
4. Arnold Engineering Development Center Arnold Air Force Base, Tenn. 37389 An Air Force Materiel Command Test Facility Test Before Flight. (2002). www.arnold.af.mil
5. Augupta Pane, E., & Abdu Rahman, R. (2022). An open design for a low-cost open-loop subsonic wind tunnel for aerodynamic measurement and characterization. HardwareX, 12, e00352. https://doi.org/10.17632/hdb93dwt2x.2
6. Bak, C., Olsen, A. S., Fischer, A., Lylloff, O., Mikkelsen, R., Gaunaa, M., Beckerlee, J., Ildvedsen, S., Vronsky, T., Grasso, F., Loeven, A., Broersma, L., Akay, B., Madsen, J., Hansen, R., & Kommer, R. (2022). Wind Tunnel benchmark tests of airfoils. Journal of Physics: Conference Series, 2265(2). https://doi.org/10.1088/1742-6596/2265/2/022097
7. Bakırcı, M., Polat, R., & Tayyip Özdemir, M. (2023). Aerodynamic Analysis of NACA 4412 Airfoil with CFD for Small Scale Wind Turbine Design. GreenTech, 2023(2), 1. https://doi.org/10.5281/zenodo.10325712
8. Barlow, J. B. ., Rae, W. H. ., & Pope, Alan. (1999). Low-speed wind tunnel testing. Wiley.
9. Barlow, T., Chao, N. H., Erdman, A., Johnson, G., Keer, L., Morgan, W., Patton, E. M., Patulski, S., Reder, R. E., Rohde, S., Shah, R., White, F., Whitehead, J., Dir, M., Beardsley, C. W., Roache, P. J., Ota, T., Okamoto, Y., Yoshikawa, H., … Billet, M. L. (1994). 1996) 0. C. JONES (1995 (Vol. 116). http://www.asme.org/terms/Terms_Use.cfm
10. Book Computational fluid dynamics _ the basics with applications -- Anderson, John -- McGraw-Hill series in mechanical engineering, 1, 1995 . (1995).
11. Book Research Methodology Methods and Techniques (C R Kothari). (2004).
12. Boundary-layer theory -- Hermann Schlichting -- McGraw-Hill series in mechanical engineering, 7th ed, 1979 -- McGraw-Hill -- 9780070553347 -- fb98336c20fbe1ac73a0d3e124dc8562 -- Anna's Archive. (1979).
13. Çengel, Y. A., & Cimbala, J. M. (2018). F L U I D M E C H A N I C S FUNDAMENTALS AND APPLICATIONS FOURTH EDITION.
14. Chowdhury, I. A. (2024). State-of-the-Art CFD Simulation: A Review of Techniques, Validation Methods, and Application Scenarios. Journal of Recent Trends in Mechanics, 9(2), 45–53. https://doi.org/10.46610/jortm.2024.v09i02.005
15. David Creswell, J. (2023). Research Design Qualitative, Quantitative, and Mixed Methods Approaches Sixth Edition.
16. Fox, R. W. ., McDonald, A. T. ., & Mitchell, J. W. . (2020). Fox and McDonald's introduction to fluid mechanics. Wiley.
17. Fransisca Soetanto, M., Hartono, B., & Rizki Zuhri, M. (2023). Numerical Study of Aerodynamic Characteristics of Airflow Around NACA 0012 and NACA 4412 Airfoils at Re = 170000. In INTERNATIONAL JOURNAL OF APPLIED TECHNOLOGY RESEARCH (Vol. 2023, Issue 2). https://ijatr.polban.ac.id/
18. Genç, M. S., Koca, K., Açıkel, H. H., Özkan, G., Kırış, M. S., & Yıldız, R. (2016). Flow characteristics over NACA4412 airfoil at low Reynolds number. In EPJ web of conferences (Vol. 114, p. 02029). EDP Sciences.
19. He, R., Sun, H., Gao, X., & Yang, H. (2022). Wind Tunnel tests for wind turbines: A state-of-the-art review. In Renewable and Sustainable Energy Reviews (Vol. 166). Elsevier Ltd. https://doi.org/10.1016/j.rser.2022.112675